Original Article

SUSTAINED ANTICANCER EFFECT BY NARINGIN-LOADED ZINC OXIDE NANOPARTICLES IN HUMAN LUNG ADENOCARCINOMA A549 CELLS

LEELARANI RAVILLA [iD], LAVANYA M. [iD], PADMINI R.* [iD]

Department of Biochemistry, Vels Institute of Science, Technology and Advanced Studies, Chennai, India
***Corresponding author: Padmini R.; *Email: padmini.sls@velsuniv.ac.in**

ABSTRACT

Objective: This study aimed to design naringin-loaded zinc oxide nanoparticles (Nar-ZnO NPs) and evaluate the formulated nanoparticles (NPs) for their antioxidant and anticancer potential.

Methods: Naringin-loaded zinc oxide nanoparticles (Nar-ZnO NPs) were prepared using a modified sol-gel method with ethylenediaminetetraacetic acid (EDTA) as a capping agent. Subsequently, were characterized using dynamic light scattering (DLS), powder X-ray diffraction (PW-XRD), Fourier transform infrared spectroscopy (FT-IR), high-resolution scanning electron microscopy (HR-SEM), and Energy Dispersive X-ray analysis (EDX). Furthermore, the naringin-loaded zinc oxide nanoparticles (Nar-ZnO NPs) were evaluated for their *in vitro* free radical scavenging activity using antioxidant assays and inhibition of lipid peroxidation potential using the altered thiobarbituric acid-reactive species (TBARS) test. The cytotoxic effect of naringin-loaded zinc oxide nanoparticles (Nar-ZnO NPs) on the non-transformed Vero cell line and lung cancer A549 cell line was investigated using the (3-[4,5-dimethylthiazol-2-yl]-2,5 diphenyl tetrazolium bromide) MTT assay. Apoptosis study was conducted using the Acridine orange/Ethidium bromide (AO/EB) double staining assay, while propidium iodide (PI) stain was utilized to observe apoptotic morphological changes.

Results: The prepared naringin-loaded zinc oxide nanoparticles (Nar-ZnO NPs) were smooth and hexagonal, with an average particle size of 500 nm. The antioxidant assays demonstrated that the naringin-loaded zinc oxide nanoparticles (Nar-ZnO NPs) and ascorbic acid exhibited comparable free radical scavenging and inhibition of lipid peroxidation activity. In MTT assay, the naringin-loaded zinc oxide nanoparticles (Nar-ZnO NPs) displayed IC_{50} values of 1014.05 µg/ml for Vero cell lines and 317.51 µg/ml for A549 cells, highlighting their influence on cell viability. Remarkably, treatment of A549 cells with the Nar-ZnO NPs resulted in dose-dependent apoptotic morphological changes, as observed through (AO/EB) double staining assay and propidium iodide (PI) stain.

Conclusion: The study findings revealed that the naringin-loaded zinc oxide nanoparticles (Nar-ZnO NPs) displayed dose-dependent free radical scavenging activity, significant inhibition of lipid peroxidation, and notable anticancer properties against A549 cells.

Keywords: Naringin-loaded zinc oxide nanoparticles, Naringin, Anticancer, Antioxidant assays, Cytotoxicity

INTRODUCTION

Cancer is the second leading cause of death, claiming about 20 million lives annually [1]. Lung cancer is a predominant type and the leading cause of cancer-related deaths worldwide, as it is typically diagnosed at an untreatable stage. Smoking is the primary cause, affecting 90% of lung cancer patients. Non-small-cell lung cancer (NSCLC) and small-cell lung cancer (SCLC) are the two well-known types, with NSCLC being more prevalent globally [2]. Employing various treatments such as chemotherapy, radiotherapy, stem cell therapy, and surgical removal has improved the health and well-being of cancer patients [3]. Despite considering chemotherapy successful and widely used, it can lead to drug resistance, resulting in an increase in dosage and causing detrimental effects on healthy cells [4].

Researchers have recently explored nanotechnology to enhance the efficacy of phytochemicals as anticancer agents. Nanoparticles (NPs) offer a platform for encapsulating and delivering drugs, thereby increasing bioavailability and absorption in biological systems. Anticancer nano-phytochemicals are gaining importance due to their ability to improve drug delivery and reduce toxicity compared to traditional chemical drugs [5]. Organic nano-delivery systems include lipid-based carriers (liposomes and micelles), polymeric NPs, polymeric conjugates, and dendrimers. Inorganic NPs like ceramic NPs, carbon nanotubes, quantum dots, magnetic NPs, and metallic NPs (e. g., gold, silver, copper, and zinc NPs) are being widely used for delivering bioactive compounds [6].

In previous research, Curcumin-loaded zinc oxide nanoparticles showed good anticancer activity against rhabdomyosarcoma (RD) cells [7]. Silibinin-conjugated gold nanoparticles demonstrated excellent anticancer effects on the A549 cell line [8]. Curcumin-loaded nanoparticles also exhibited effective anticancer activity against lung cancer cell lines compared to curcumin alone [9]. Syringic acid-loaded zinc oxide nanoparticles revealed anticancer activity against lung cancer both *in vitro* and *in vivo* [10].

Naringin [5,7-trihydroxyflavanone-7—D—L-rhamnosyl[1→2]—D-glucoside] is a natural flavanone glycoside that is abundant in citrus fruits, primarily grapefruit and sour orange, as well as in tomatoes and other fruits. Naringin is described as having antioxidant, antibacterial, anti-inflammatory, anti-apoptotic, and antimutagenic properties [11]. Despite its pharmacological properties, naringin has low oral bioavailability, limiting its therapeutic applications. Therefore, to increase its bioavailability, in this study, we described the Naringin-encapsulated nanoparticle. To enhance bioavailability, we developed naringin-encapsulated zinc oxide (ZnO) nanoparticles. ZnO nanoparticles are preferred due to low toxicity, biodegradability, and affordability. Additionally, they exhibit targeted anticancer potential [12, 13].

According to the literature review, naringin-loaded zinc oxide nanoparticles are not yet been developed. In this study, our focus was on fabricating and characterizing naringin-loaded zinc oxide nanoparticles (Nar-ZnO NPs) while investigating *in vitro* free radical scavenging activity, lipid peroxidation inhibition, as well as examining their cytotoxic effects and apoptotic induction on Vero and A549 cells.

MATERIALS AND METHODS

Chemicals

We procured naringin from Sigma Aldrich in the United States. The other compounds utilized in the investigation were all of analytical quality.

Cell line and culture

A549 (human lung cancer cell) and VERO (normal monkey kidney cell) were procured from the National Centre for Cell Science, Pune, India (NCSS) and were used to assess the anticancer cell activity and cytotoxicity against synthesized Nar-ZnO NPs. The cells were maintained in Minimal Essential Media supplemented with 10% FBS, 100 U/ml of penicillin, and 100 µg/ml of streptomycin at 37 °C in a humidified environment with 5% CO_2.

Preparation of naringin-loaded zinc oxide nanoparticles

To modify the sol-gel method [14] for producing ZnO NPs, we utilized ethylenediaminetetraacetic acid (EDTA) as a capping agent. The process included dissolving 200 mg naringin in 100 ml of ethanol and stirring the solution to achieving even mixing. A mixture of Zinc acetate dihydrate and NaOH, heated to 60-80 °C and constantly stirred, slowly received the addition of this solution. Subsequently, we introduced 0.04 M EDTA and dropwise added 100 ml of ethanol over 90 min while vigorously stirring the mixture, resulting in the formation of a gel-like substance. The mixture was incubated overnight at 60 °C and then calcined for 4 h at 150 °C. The nanoparticles (NPs) that resulted were washed with ethanol, decanted, and calcined once more for an hour to obtain a fine powder.

Physical and physico-chemical characterization

Particle size analysis and polydispersity Index measurement

The Nanotrac Wave II Particle Size Analyzer was utilized to ascertain the particle size of ZnO NP samples. Prior to the analysis, the samples were diluted by ten times with Milli-Q water. The samples were also examined for hydrodynamic radius, Polydispersity Index (PDI), and zeta potential. The particles were suspended in water as a dispersion medium and normal saline with a pH of 7.4. To ensure sample homogeneity, it is vital to assess the Polydispersity Index (PDI) of NPs.

Powder X-ray diffraction

The interfacial properties, size, and crystal structure of ZnO NPs were examined using an X-ray diffractometer (PAN analytical X'Pert PRO). A diffraction pattern was obtained using CuKα radiation with a wavelength of 1.541 A°. To produce a thin film of the sample for XRD analysis, a small amount was spread onto a glass plate. The scanning was performed within the 2θ value range of 4° to 80°, with a time constant of 0.02 min^{-1} and 1 sec. The instrument was set to run at 40 kV Voltage and 30 mA current. Scherrer's equation was utilized to determine the median grain size of the synthetic nanoparticles, as shown below.

$$Dp = \frac{0.9\lambda}{\beta Cos\theta}$$

Where D defines the size of the crystallite, λ denotes the wavelength (1.5406 for Cu Kα), FWHM represents the primary intensity peak's full width at half maximum (FWHM) after subtracting equipment broadening and θ serves as a diffraction angle in radians.

Fourier transmission Infrared Spectroscopy (FT-IR)

The surface chemistry of NPs was examined using FT-IR spectroscopy, which revealed the functional groups attached to the NP surfaces in the 4000-400 cm^{-1} range. The samples were prepared by uniformly dispersing ZnO nanoparticles in a dry KBr matrix and crushing it to form a clear disc.

Scanning electron microscopy (SEM) with energy-dispersive x-ray analysis (EDX)

The morphological evaluation of the naringin–loaded Zinc oxide nanoparticles (Nar-ZnO NPs) samples was conducted using a field emission scanning electron microscope (JEOL, Model: JSM-7600F) in the range of 0.1 nm to 10,000 nm. The data collected from all approaches were analysed using Origin software version 9.1.

Determination of free radical scavenging activity

1, 1-Diphenyl-2-picrylhydrazyl [DPPH] free radical-scavenging activity

The radical scavenging capacity of Nar-ZnO NPs at different concentrations was assessed using the DPPH assay [15]. A 0.1 mmol DPPH solution was prepared by dissolving 4 mg of DPPH in 100 ml of ethanol. Nar-ZnO NPs extracts of various volumes (2-20 ml) were prepared using DMSO and added to 2.96 ml of the DPPH solution. The mixture was then incubated in the dark at room temperature for 20 min, and the absorbance was measured at 517 nm to determine the scavenging effect percentage. In control, the sample's volume was substituted with the same amount of solvent. A graph of the scavenging effect percentage versus sample concentrations was used to determine the IC_{50} (the sample concentration that provides 50% inhibition). The samples' radical scavenging activity (% RSA) was estimated using the formula below:

$$\% \text{ RSA} = \frac{[\text{Abs control} - \text{Abs sample}]}{\text{Abs control}} \times 100$$

Where Abs control is the absorbance of DPPH radical+ethanol,

Abs sample is the absorbance of DPPH radical+sample.

The sample concentration that provides 50% inhibition (IC_{50}) was calculated from that graph.

2,2'-Azino-bis[3-ethylbenzothiazoline-6-sulphonic acid [ABTS] radical scavenging assay

The ABTS radical cation decolorization assay was performed to evaluate the synthesized NPs' ability to scavenge free radicals [15]. To generate the ABTS cation radical, 7 mmol ABTS was mixed with 2.45 mmol potassium persulfate [1:1] in water and incubated in the dark at room temperature for 12 to 16 h. The resulting $ABTS^+$ solution was then diluted with methanol to achieve an absorbance of 0.700 at 734 nm. Next, 3.995 ml of the diluted $ABTS^+$ solution was mixed with 5 µl of the sample, and the absorbance was measured 30 min later. The percentage inhibition of absorbance at 734 nm was calculated using the formula.

$$\text{ABTS + RSA \%} = \frac{[\text{Abs control} - \text{Abs sample}]}{\text{Abs control}} \times 100$$

Where Abs control is the absorbance of $ABTS^+$radical+ethanol, Abs sample is the absorbance of $ABTS^+$radical+sample.

IC_{50} value was determined from that graph as described in the DPPH method.

Phosphomolybdenum assay

The formation of the green phosphomolybdenum complex was used to measure the antioxidant activity of the samples [16]. To create the phosphomolybdate reagent, 0.588 ml of sulphuric acid, 0.049 g of ammonium molybdate, and 0.036 g of sodium phosphate were combined and made up to a final volume of 10 ml using distilled water. Then, 1 ml of the Nar-ZnO DMSO solution was mixed with 1 ml of the phosphomolybdate reagent, and the mixture was incubated at 95 °C for 90 min in a boiling water bath. The absorbance was then measured at 695 nm. Ascorbic acid (10 mg/ml DMSO) was used as a standard, and the IC_{50} value was determined graphically.

$$\text{PRP\%} = \frac{[\text{Abs control} - \text{Abs sample}]}{\text{Abs control}} \times 100$$

Ferric reducing antioxidant power (FRAP)

To determine the FRAP percentage, the bluish-colored complex was measured colorimetrically using Oyaizu's method with slight modifications [17]. A 0.2 M phosphate buffer with a pH of 6.6 was prepared using monobasic sodium phosphate and dibasic sodium phosphate. In addition, 0.1% ferric chloride, 10% trichloroacetic acid [TCA], and 1% potassium ferricyanide were also prepared. Further, 2.5 ml of the ferricyanide solution was mixed with 1 ml of the sample solution and 2.5 ml of the phosphate buffer and then incubated at 50 °C for 20 min. After centrifuging the mixture and removing the upper 2.5 ml of the supernatant, 2.5 ml of 10% TCA was added and mixed. Finally, the remaining 2.5 ml supernatant was mixed with 0.5 ml of $FeCl_3$, and the absorbance was measured at 700 nm. A higher absorption indicates stronger antioxidant activity.

$$\% \text{ FRAP} = \frac{[\text{Abs control} - \text{Abs sample}]}{\text{Abs control}} \times 100$$

IC_{50} value was determined graphically as reported in the DPPH method.

Lipid peroxidation assay

The extent of lipid peroxidation was measured using an altered thiobarbituric acid-reactive species (TBARS) test [18] with egg yolk homogenates as a lipid-rich medium. Malondialdehyde and two molecules of TBA were added to the test, producing a pinkish-red chromogen with maximum absorbance at 532 nm. A mixture of 1.0 ml of distilled water, 50 µl of the sample, and 250 µl of egg homogenate (10%, v/v in distilled water) was placed in a test tube. Then, 25 µl of FeSO4 (0.075 M) was added, and the mixture was incubated for 30 min to cause lipid peroxidation. After that, 750 ml of 0.8% TBA (w/v) produced in 1.1% sodium dodecyl sulfate and 25 ml of 20% acetic acid (pH 3.5) was added to the 20% TCA and mixed thoroughly. The mixture was boiled for 60 min in a water bath. Each tube was filled with 3.0 ml of butanol and allowed to cool before centrifugation at 3000 rpm for 10 min. The absorbance of the organic top layer was measured at 532 nm against 3 ml of butanol. The blank was substituted with 50 µl of distilled water. The inhibition of lipid peroxidation was calculated using the following equation:

$$\% \text{ Inhibition } = \frac{[\text{Abs control} - \text{Abs sample}]}{\text{Abs control}} \times 100$$

The concentration of sample inhibiting 50 % lipid peroxidation was calculated graphically as described in the DPPH method.

Determination of anticancer activity against VERO and A549 cell lines

Cytotoxicity by (3-[4,5-dimethylthiazol-2]-2,5-diphenyltetrazolium bromide) MTT assay

A live cell's ability to convert (3-[4,5-dimethylthiazol-2]-2,5-diphenyltetrazolium bromide) MTT into formazan dyes served as the basis for the experiment [19]. A colorimetric approach was used in the assay to quantify cell viability. At 37 °C in 5% CO_2 incubator, 96-well microplates with 1×10^6 cells per well were seeded with the VERO and A549 cell lines. After reaching 90% confluence, the medium was then changed, and the cell lines were treated with samples of various concentrations (50, 100, 200, 400, and 500 µg) and incubated for 24 h. After washing the cells with phosphate buffer saline (PBS, pH 7.4), 20 µl of the MTT solution (5 mg/ml) was added. The plates were then positioned in the dark at 37 °C for 4 h. After the formazan crystals were dissolved in 100 ml DMSO, the absorbance was measured spectrophotometrically at 570 nm. The following equation was used to express the percentage of cell viability:

$$\% \text{ cell viability} = \frac{\text{Absorbance of treated cells}}{\text{Absorbance of control cells}} \times 100$$

The IC_{50} value is commonly used as a criterion in cytotoxicity studies and is defined as the concentration at which 50% of cell growth is inhibited. After 24 h, the morphologies of both the untreated (control) and treated cells were examined and photographed under a bright field microscope.

Determination of apoptosis

Propidium Iodide (PI) staining was used to detect apoptosis in A549 cells. PI binds to nucleic acids by intercalating between the nitrogenous bases. PI is a fluorescent molecule that stains apoptotic nuclear modifications. Acridine orange/Ethidium bromide (AO/EB) dual labelling was used to examine the effects of apoptosis-related changes induced by Nar-ZnO NPs in A549 cells [20]. In contrast to EB stain, which has only been absorbed by nonviable cells and causes them to lose the stability of their membrane, AO stain is absorbed by both viable and nonviable cells and emits green fluorescence. The IC_{50} concentration of Nar-ZnO NPs was applied to A549 Cells, which were grown in a 6-well plate (1×10^5 cells per well), for 24 h. Cells left untreated served as the control. The treated cells were rinsed with PBS before being stained for 5 min with 10 µl of PI stain and 20 µl of an AO/EB staining solution (100 g/ml AO and 100 g/ml EB). Stained cells were observed using a fluorescent microscope with 40x magnification.

Statistical analysis

Statistical analysis was performed using Microsoft Excel spreadsheet. The calculation of standard deviation was carried out using the formula STDEV. S.

RESULTS AND DISCUSSION

In the current study, Nar-ZnO nanoparticles were prepared using a sol-gel process with slight modifications. To improve the stability of the nanoparticles, limit their size and prevent their growth, we used EDTA as the capping agent. We combined Zinc oxide capped with EDTA with naringin in an ethanol solvent to enhance the antioxidant and anticancer properties of naringin in the prepared Nar-ZnO nanoparticles.

Synthesis and characterization of naringin-loaded ZnO nanoparticles

Various techniques have been described in the scientific literature for synthesizing Zinc oxide nanoparticles, including hydrothermal treatment, microwave synthesis, ultrasound, and the sol-gel method. Among these methods, the sol-gel method has garnered significant interest due to its advantages in terms of accessibility for biological activity and quantification. It is favoured for its simplicity, reliability, reproducibility, and cost-effectiveness compared to other synthesis methods. Naringin-loaded zinc oxide nanoparticles were successfully synthesized and demonstrated remarkable stability even when stored at room temperature (fig. 1). The synthesized nanoparticles exhibited excellent stability over extended periods, retaining their structural integrity and desired properties. This stability at ambient conditions is highly advantageous for their practical applications, as it ensures the long-term viability and efficacy of the nanoparticles. The robust stability observed at room temperature further highlights the potential of these Nar-ZnO NPs for various biomedical, pharmaceutical, and industrial applications, where stability is a critical factor.

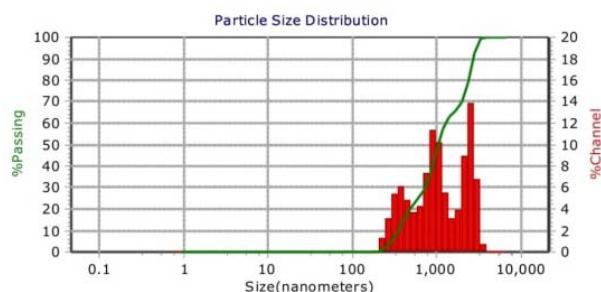**Fig. 1: Naringin-loaded ZnO nanoparticles**

Fig. 2: Particle size analysis by dynamic light scattering technique

Particle size analysis and polydispersity index (PDI) measurement

The particle size of the synthesized nanoparticle is presented in (fig. 2). The Nar-ZnO NPs exhibited a zeta potential of +200mV

and a particle size ranging from 200 to 800 nm, with a polydispersity index (PDI) of 0.59. In a 2016 study by K. Pate [21], it was reported that a zeta potential stability range greater than 60 demonstrated excellent stability. Therefore, the zeta potential provides valuable information on the stability of the synthesized NPs. The higher the zeta potential, irrespective of charge, the more stable the NPs. The positive zeta potential of 200 mV aids in the chemical stability of products with low water solubility by preventing negatively charged ions from being adsorbed onto their surface and interfering [22]. The synthesized NPs have varying sizes due to their high PDI and outstanding stability at room temperature.

Powder XRD

The X-ray diffraction analysis allowed for the determination of crystal lattices and particle sizes. Prominent diffraction peaks were observed for lattice planes [1 0 0], [0 0 2], [1 0 1], [1 0 2], [1 0 0], [1 0 3], [2 0 0], [1 1 2], and [2 0 1] at corresponding 2θ values of 31.962°, 34.586°, 36.414°, 47.620°, 51.754°, 62.982 °, and 68.06° (fig. 3). These peaks were attributed to the hexagonal phase of ZnO, consistent with previous research [23] and matching the JCPDS file: 36-1451. The mean crystallite size of zinc was determined to be 15.22 nm using Scherrer's equation, based on the full width at half maximum (FWHM) of the peak corresponding to the 101 planes at 36.26°, which exhibited higher intensity.
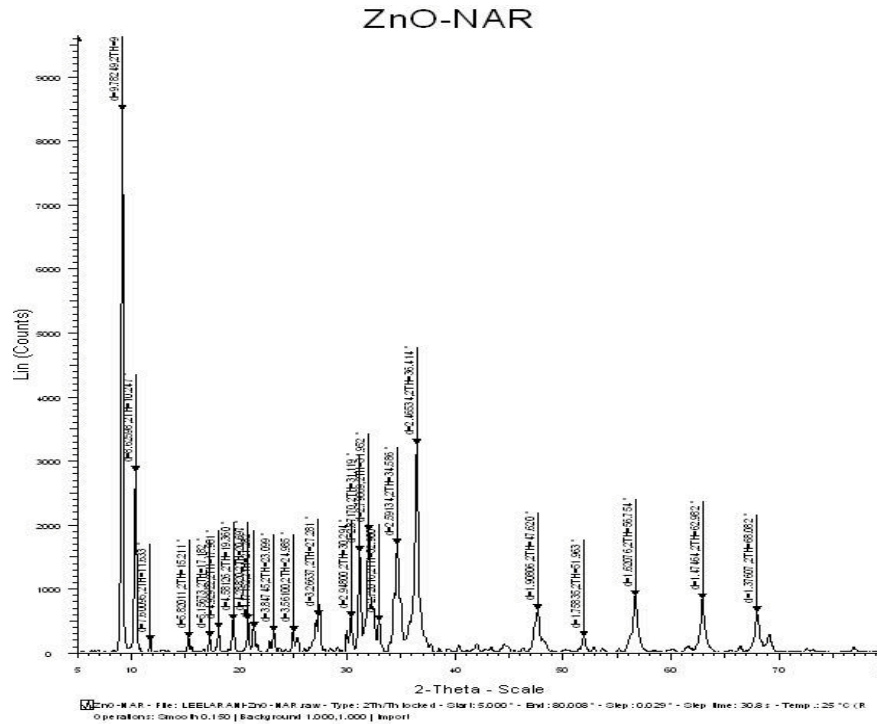

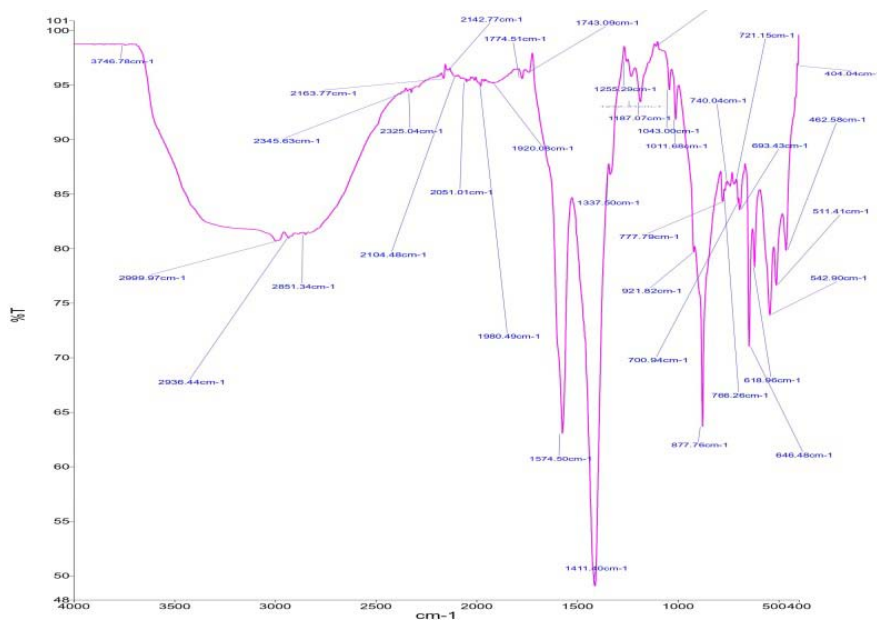Fig. 3: XRD pattern depicting d values varying with 2θ range from 0° to 80°

Fig. 4: FT-IR spectrum of naringin-loaded ZnO NPs

FT-IR analysis

Fig. 4 illustrates the FT-IR absorption spectra of synthesized Nar-ZnO NPs. The peaks in the region of 550 cm^{-1} and 400 cm^{-1} contain the unique peaks of ZnO-NPs [24], while several sharp peaks between 1700 cm^{-1} and 1000 cm^{-1} represent naringin. The spectra indicated the existence of bonds due to O–H stretching around 3,430 cm^{-1}, the large peak from 3500–3000 cm^{-1} and aldehydic C–H stretching around 2,920 cm^{-1} [24]. These findings align with those of M. M. AbdElhady (2012) [25], who reported the presence of zinc oxide nanoparticles at a stretching peak of 465 cm^{-1} in chitosan/zinc oxide nanoparticles. Therefore, the FTIR study suggests that the OH group of naringin binds to the zinc oxide group of synthesized nanoparticles.

HR-SEM and EDX

The hexagonal structure of the Nar-ZnO NPs was observed using HR-SEM images at a magnification of 60,000x as shown in fig. 5. This is consistent with the findings of a previous study by P. K. Giri *et al.*, (2012) [26], which also showed the hexagonal shape of zinc oxide nanoparticles. The EDX spectral analysis confirmed the presence of zinc and oxygen in the synthesized nanoparticle. The result of the EDX study indicating a zinc content of 5.28% and an oxygen content of 42.0% in the Nar-ZnO NPs (fig. 7A, 7B).
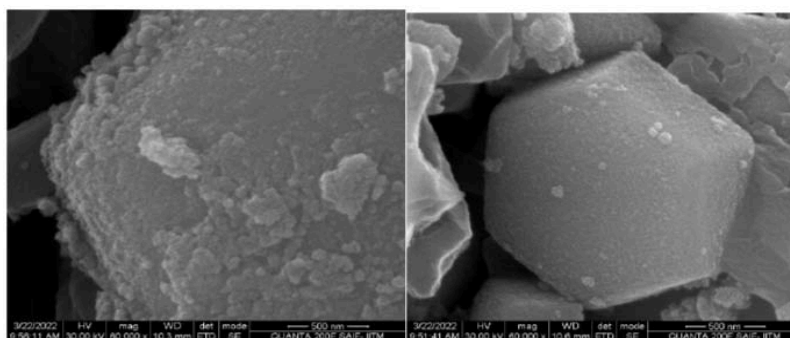

Fig. 5: HR-SEM images of naringin-loaded ZnO NPs at 60,000 X magnification
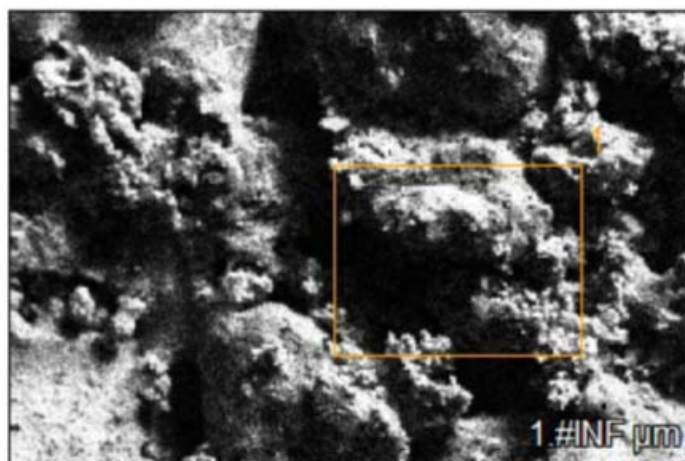

Fig. 6: EDX image of naringin-loaded ZnO NPs

Net Counts

	C	O	Al	Si	Zn
Base(25)_pt1	2449	24510	281	3486	14941

Weight %

	C	O	Al	Si	Zn
Base(25)_pt1	7.08	31.98	0.19	1.78	16.45

Weight % Error (+/- 1 Sigma)

	C	O	Al	Si	Zn
Base(25)_pt1	±0.14	±0.23	±0.03	±0.05	±0.31

Atom %

	C	O	Al	Si	Zn
Base(25)_pt1	12.38	42.00	0.15	1.34	5.28

Atom % Error (+/- 1 Sigma)

	C	O	Al	Si	Zn
Base(25)_pt1	±0.24	±0.30	±0.02	±0.04	±0.10

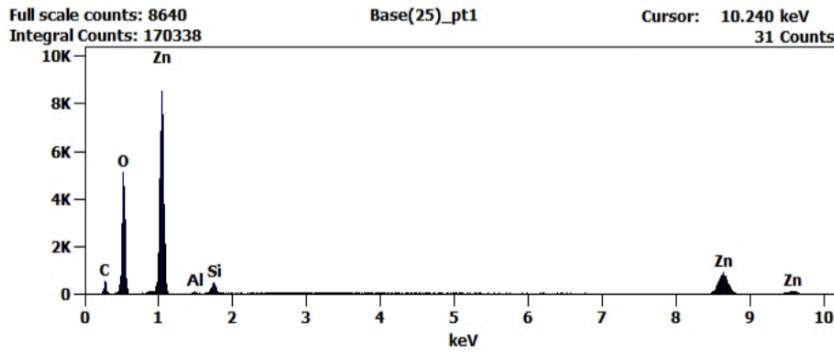Fig. 7A: EDX elemental analysis of the naringin-loaded ZnO NPs

Fig. 7B: EDX elemental analysis of the naringin-loaded ZnO NPs

Free radical scavenging activity

Free radical chain reactions are a major factor in the pathogenesis of many diseases. These highly reactive and electrophilic moieties can cause oxidative damage by reacting with lipids, proteins, and nucleic acids, leading to the manifestation of their toxic effects [27]. Cancer and cardiovascular diseases are strongly associated with increased free radical production. Free radical chain reactions initiating lipid peroxidation are associated with the damage of biomembranes in cells. Several studies have demonstrated that protecting against free radical damage to cellular DNA, lipids, and proteins, as well as supplementing with dietary antioxidants, can reduce oxidative stress and prevent or delay the development of disease-related complications [28, 29]. In the current study, the scavenging abilities of synthesized Nar-ZnO NPs against DPPH free radicals, ABTS+free radicals, PRP, FRAP, and lipid peroxidation (table 1). Our findings indicated an increasing concentration-dependent antioxidant potential. The IC_{50} values for the assays mentioned above were calculated using a graphical technique. Results revealed that naringin–loaded Zinc oxide nanoparticles (Nar-ZnO NPs) exhibited significant lipid peroxidation inhibition at low concentrations. The produced NPs showed improved antioxidant and lipid peroxidation inhibitory properties in a dose-dependent manner. The higher concentrations of Nar-ZnO NPs are found to be more potent antioxidants. When compared to the same concentrations of standard ascorbic acid, Nar-ZnO NPs showed significant antioxidant activity. Additionally, these NPs inhibited lipid peroxidation to a significant extent. Similar antioxidative action has been observed for naringin [30] and zinc oxide nanoparticles from *Luffa acutangula* peel extract [31]. Therefore, we conclude that NAR-ZnO nanoparticles have great potential for therapeutic use in combatting oxidative stress due to their ability to scavenge free radicals effectively.

Table 1: *In vitro* antioxidant analysis of Nar-ZnO NPs

Concentration [µg/ml]	DPPH RSA %		ABTS RSA %		% PRP		% FRAP		% Inhibition of lipid peroxidation	
	Sample	Standard	Sample	Standard	Sample	Standard	Sample	Standard	Sample	Standard
20	25.12±0.87	27.71±1.12	23.73±0.73	24.32±1.26	24.84±1.74	21.12±1.63	23.73±2.34	27.12±1.93	26.12±0.33	27.32±1.25
40	54.27±1.37	46.23±1.1	46.53±2.13	47.13±1.92	38.68±1.43	41.63±1.22	48.57±1.13	49.83±0.75	44.53±1.84	48.14±1.12
60	66.63±1.84	76.18±1.45	67.34±2.53	78.16±2.54	59.51±1.88	67.32±1.46	74.74±2.67	79.32±2.47	76.32±2.13	80.26±2.64
80	82.63±3.92	89.34±3.32	83.33±2.61	92.32±2.31	71.48±2.32	83.14±2.12	87.61±2.64	93.15±2.14	93.21±3.13	94.14±3.94
IC_{50} value [µg/ml]	42.24	40.81	44.75	41.07	51.70	46.87	42.04	39.14	41.37	39.28

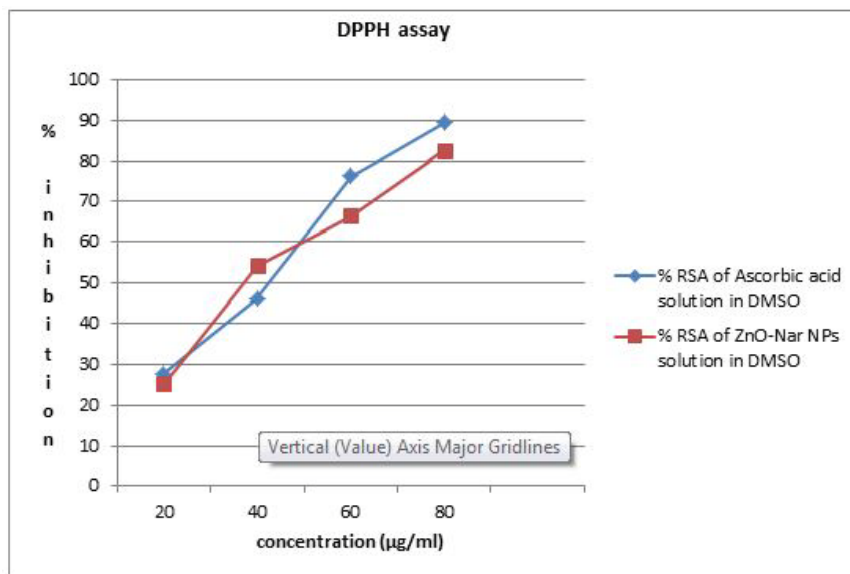Note: Results are expressed as mean±SD (n=5)

Fig. 8: (DPPH) free radical-scavenging activity of different concentrations of synthesized NPs in comparison with ascorbic acid
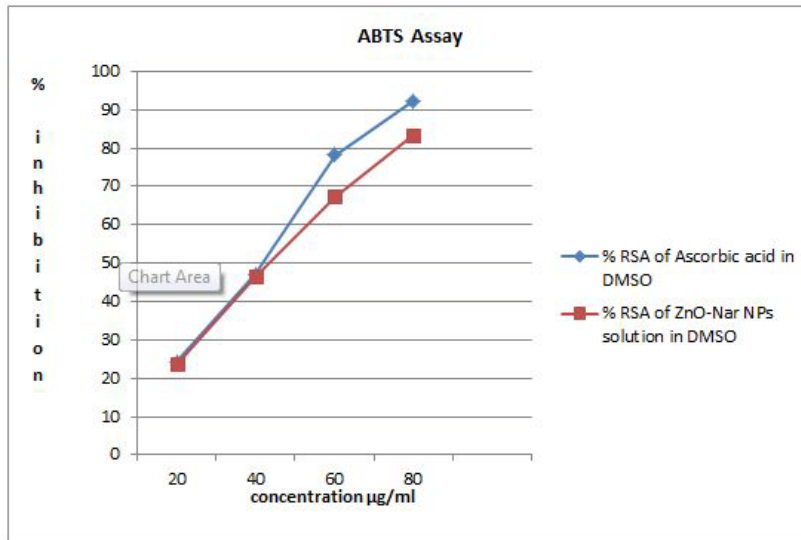
Fig. 9: ABTS⁺radical-scavenging activity of different concentrations of synthesized NPs in comparison with ascorbic acid
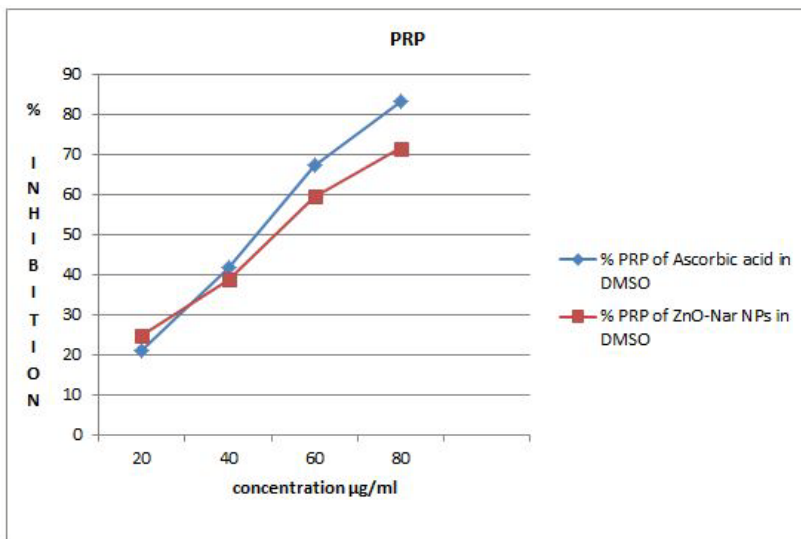

Fig. 10: Phosphomolybdenum reduction potential (PRP) of different concentrations of synthesized NPs in comparison with ascorbic acid
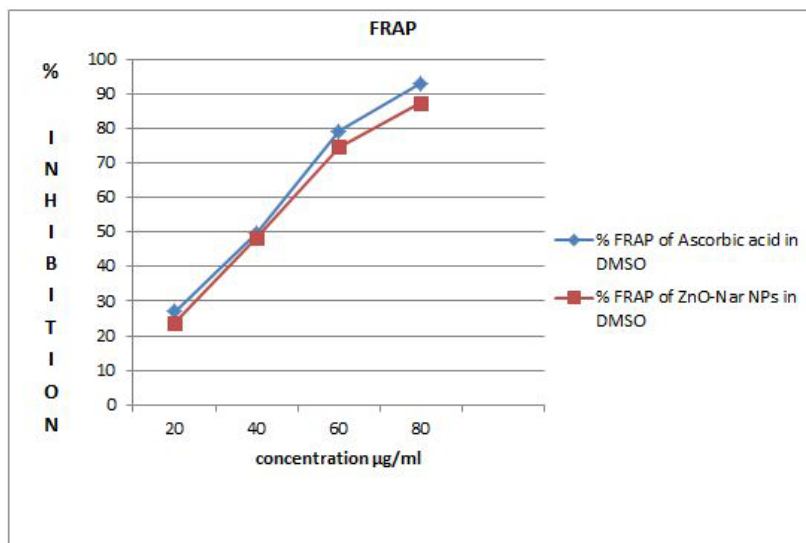

Fig. 11: Ferric reducing antioxidant power (FRAP) of different concentrations of synthesized NPs in comparison with ascorbic acid
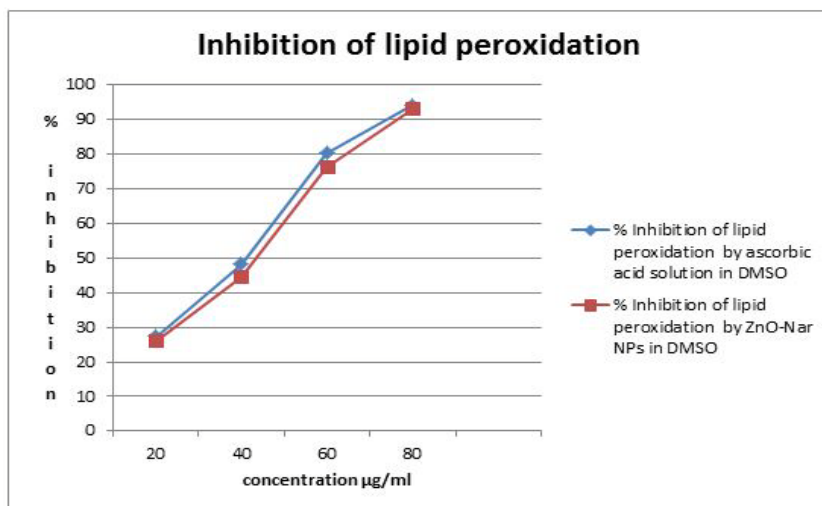
Fig. 12: Inhibition of lipid peroxidation by different concentrations of synthesized NPs in comparison with ascorbic acid

Cell viability and anticancer activity against cell lines

The determination of cell viability is a crucial parameter for monitoring the response to cytotoxic drugs. The results of the MTT assay showed a dose-dependent reduction in cell viability in A549 cells, becoming significant at concentrations of 100 μg/ml and higher (table 2), while having little effect on Vero cells at the same concentration. The IC_{50} values of Nar-ZnO NPs on non-transformed Vero cell lines and cancerous A549 cell lines showed a significant difference, indicating its potential as an anticancer drug. The reduction of tetrazolium salts to formazan dyes could contribute to the decrease in mitochondrial dehydrogenase activity. This decrease in the ability of tetrazolium salts to be reduced into formazan dyes might result in a decline in mitochondrial dehydrogenase activity [32]. The cytotoxic effects on A549 cells were analyzed using Acridine orange/Ethidium bromide (AO/EB) double staining assay. Both A549 and Vero cells were exposed to naringin-loaded ZnO NPs at various concentrations ranging from 100 to 1000 μg/ml for 24 h to determine its cytotoxicity effect on the cells. Nar-ZnO NPs did not show a cytotoxic effect on Vero cells (fig. 14), as per the results of the cytotoxicity assay. However, A549 cells were found to be sensitive at a concentration 500 μg/ml (table 2). The results (fig. 16) revealed a significant decrease in A549 cell viability, as indicated by LDH release in the Nar-ZnO NPs group compared to the control group. Furthermore, the appearance of apoptotic cells and the release of LDH enzymes were dose-dependent. Continuous exposure of A549 cells to the IC_{50} concentration of naringin-loaded zinc oxide nanoparticles led to increased LDH release, resulting in cell death (fig. 16c). Cell death can be categorized into

apoptosis and necrosis. Apoptosis is the orderly dismantling and removal of damaged cells, while necrosis is an uncontrolled breakdown of cells where the leaked cellular debris leads to an inflammatory reaction [33]. During apoptosis, the cell membrane remains intact, but the cytoplasm condenses, and the nucleus breaks up into DNA fragments. Cells undergoing necrosis possess damaged membranes and consequently bind to the propidium iodide dye, resulting in a red-pink appearance (fig. 16e). A549 cells treated with naringin-loaded zinc oxide (Nar-ZnO NPs) nanoparticles showed an increased absorption of the dye propidium iodide, which was concentration-dependent. The nanoparticles could adhere to cellular protrusions and fuse with the plasma membrane. The results also showed an increase in early apoptotic cells stained with fluorescent green and late apoptotic cells with bright orange patches of condensed chromatin in the nucleus that distinguished them from necrotic cells with orange-reddish fluorescence (fig. 16f). The results discussed above were consistent with earlier research, which demonstrated that biogenic ZnO NPs had potent cytotoxic effects on the A549 lung cancer cell line [34]. Jolita Stabrauskiene *et al.*, (2022) reported that naringin exerted its cytotoxic effects by inducing oxidative stress (ROS) in cancer cells, which disrupts mitochondrial membrane potential and ultimately leads to cell death/apoptosis [35]. In the current study, it was found that naringin-loaded zinc oxide nanoparticles increased the number of apoptotic cells and LDH release in A549 cells, demonstrating cytotoxic effects on human lung cells. The effect was found to be dose-dependent. The unique physicochemical properties and high specific surface area-to-volume ratios of nanoparticles are primarily responsible for their diverse antioxidant and anticancer capabilities.
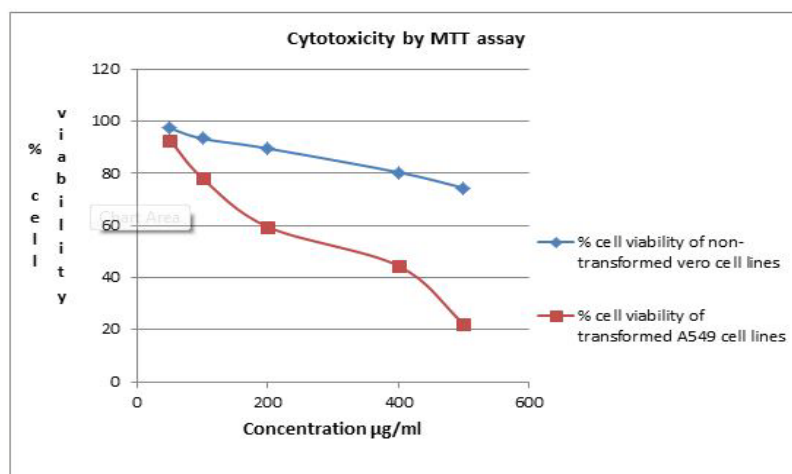

Fig. 13: MTT assay of VERO and A549 cell lines treated with different concentrations of naringin-loaded ZnO NPs

Table 2: % cell viability of vero and A549 cell lines after treating with Nar-ZnO NPs

Concentration µg/ml	% cell viability of non-transformed Vero cell lines	% cell viability of transformed A549 cell lines
Control	100	100
50	97.38±0.58	92.86±1.09
100	93.41±0.52	78.22±0.84
200	89.63±0.65	59.53±0.15
400	80.48±1.15	44.56±0.23
500	74.49±0.13	22.23±0.10
IC50 value [µg/ml]	1014.05	317.51

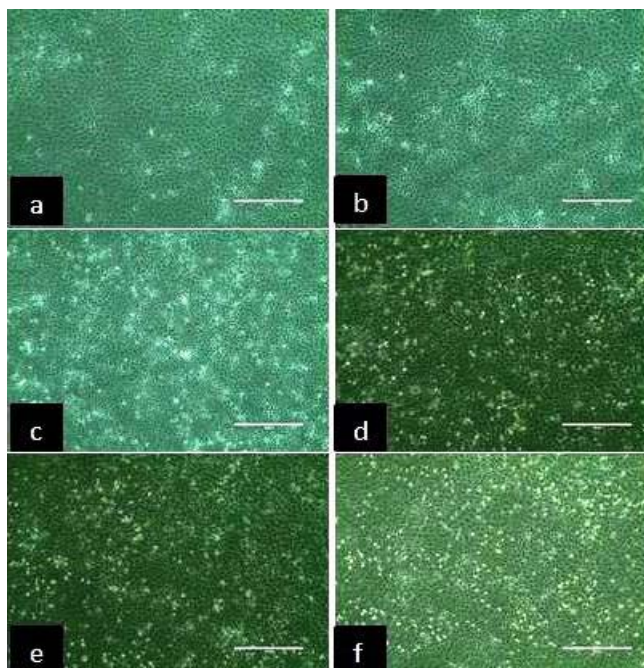Note: Results are expressed as mean±SD (n=3)

Fig. 14: MTT assay images of Vero cell lines treated with different concentration of naringin-loaded ZnO NPs: (a) Vero cell line control (b) Treated with 50 µg Nar-ZnO NPs (c) Treated with 100 µg Nar-ZnO NPs (d) Treated with 200 µg Nar-ZnO NPs (e) Treated with 400 µg Nar-ZnO NPs (f) Treated with 500 µg Nar-ZnO NPs
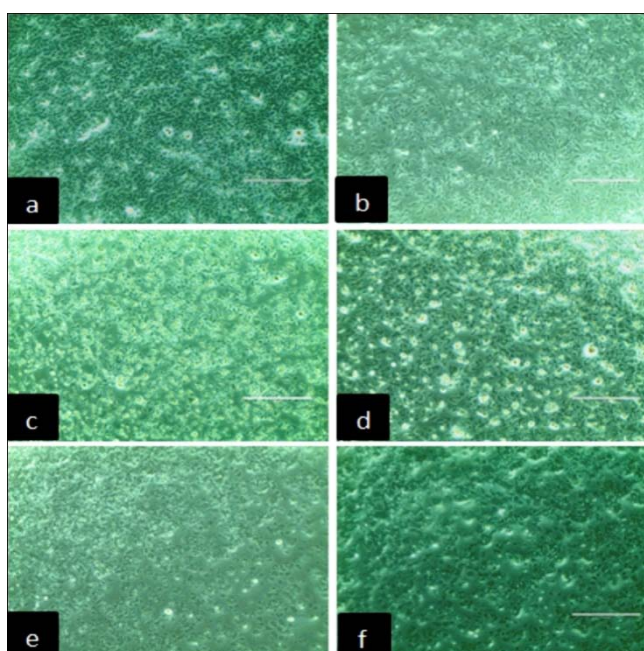

Fig. 15: MTT assay images of A549 cell lines treated with different concentration of naringin-loaded ZnO NPs (a) A549 cell line control (b) Treated with 50 µg Nar-ZnO NPs (c) Treated with 100 µg Nar-ZnO NPs (d) Treated with 200 µg Nar-ZnO NPs (e) Treated with 400 µg Nar-ZnO NPs (f) Treated with 500 µg Nar-ZnO NPs
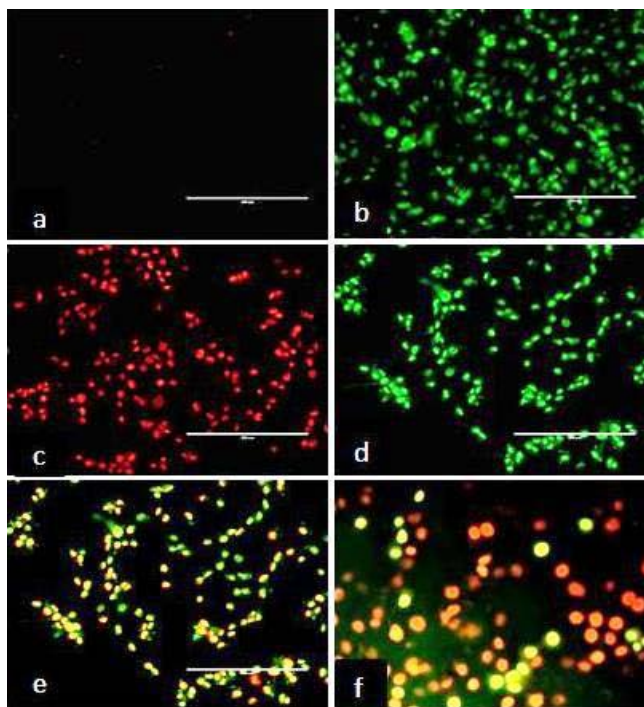
Fig. 16: AO/EB staining and PI staining to study apoptosis

CONCLUSION

The synthesized naringin-zinc oxide nanoparticle has an effective antioxidant potential. The naringin-zinc oxide nanoparticle, when exposed to the A549 lung cancer cell line, exhibited a dose-dependent cytotoxic effect, demonstrating its excellent anticancer potential. Therefore, the study concluded that encapsulating naringin with Zinc oxide nanoparticles enhances its anticancer potential. This study represents the first exploration of the anticancer potential of naringin-loaded zinc oxide nanoparticles. In the future, the research could extend to *in vivo* experiments, aiming to determine their effectiveness in enhancing the quality of life for cancer patients.

AUTHORS CONTRIBUTIONS

All authors gave unanimous approval of the version to be published, consented to submit the article to the current journal, contributed significantly to the data analysis and interpretation, agreed to be held answerable for all aspects of the work, and participated in its drafting or critical revision for important intellectual content.

CONFLICTS OF INTERESTS

The authors declare that there are no conflicts of interest.

REFERENCES

1. Sung H, Ferlay J, Siegel RL, Laversanne M, Soerjomataram I, Jemal A. Global cancer statistics 2020: globocan estimates of incidence and mortality worldwide for 36 cancers in 185 countries. CA Cancer J Clin. 2021 May;71(3):209-49. doi: 10.3322/caac.21660, PMID 33538338.
2. Hu C, Du W. Zinc oxide nanoparticles (ZnO NPs) combined with cisplatin and gemcitabine inhibits tumor activity of NSCLC cells. Aging (Albany, NY). 2020 Dec 20;12(24):25767-77. doi: 10.18632/aging.104187, PMID 33232271.
3. Meyers CA. How chemotherapy damages the central nervous system. J Biol. 2008;7(4):11. doi: 10.1186/jbiol73, PMID 18439322.
4. Mishra P, Ahmad A, Al-Keridis LA, Alshammari N, Alabdallah NM, Muzammil K. Doxorubicin-conjugated zinc oxide nanoparticles, biogenically synthesized using a fungus Aspergillus niger, exhibit high therapeutic efficacy against lung cancer cells. Molecules. 2022 Apr 16;27(8):2590. doi: 10.3390/molecules27082590, PMID 35458790.
5. Ashraf MA. Phytochemicals as potential anticancer drugs: time to ponder nature's bounty. BioMed Res Int. 2020 Mar 6;2020:8602879. doi: 10.1155/2020/8602879, PMID 32076618.
6. Enrico CE. Nanotechnology-based drug delivery of natural compounds and phytochemicals for the treatment of cancer and other diseases. Stud Nat Prod Chem. 2019;62:91-123. doi: 10.1016/B978-0-444-64185-4.00003-4.
7. Perera WPTD, Dissanayake RK, Ranatunga UI, Hettiarachchi NM, Perera KDC, Unagolla JM. Curcumin-loaded zinc oxide nanoparticles for activity-enhanced antibacterial and anticancer applications. RSC Adv. 2020;10(51):30785-95. doi: 10.1039/D0RA05755J, PMID 35516060.
8. Ravi R, Zeyaullah M, Ghosh S, Khan Warsi MK, Baweja R, AlShahrani AM. Use of gold nanoparticle-silibinin conjugates: a novel approach against lung cancer cells. Front Chem. 2022 Oct 19;10:1018759. doi: 10.3389/fchem.2022.1018759, PMID 36311430.
9. Yin H, Zhang H, Liu B. Superior anticancer efficacy of curcumin-loaded nanoparticles against lung cancer. Acta Biochim Biophys Sin (Shanghai). 2013 Aug;45(8):634-40. doi: 10.1093/abbs/gmt063, PMID 23786839.
10. Yang N, Qiu F, Zhu F, Qi L. Therapeutic potential of zinc oxide-loaded syringic acid against *in vitro* and *in vivo* model of lung cancer. Int J Nanomedicine. 2020 Oct 27;15:8249-60. doi: 10.2147/IJN.S272997, PMID 33149573.
11. Salehi B, Fokou PVT, Sharifi Rad M, Zucca P, Pezzani R, Martins N. The therapeutic potential of naringenin: a review of clinical trials. Pharmaceuticals (Basel). 2019 Jan 10;12(1):11. doi: 10.3390/ph12010011, PMID 30634637.
12. Lakshmipriya T, Gopinath SCB. Introduction to nanoparticles and analytical devices. Nanoparticles Anal Devices. 2021:1-29. doi: 10.1016/B978-0-12-821163-2.00001-7.
13. Rani N, Rawat K, Saini M, Shrivastava A, Kandasamy G, Saini K. Rod-shaped ZnO nanoparticles: synthesis, comparison and in vitro

evaluation of their apoptotic activity in lung cancer cells. Chem Pap. 2022;76(2):1225-38. doi: 10.1007/s11696-021-01942-y.

14. Singh G, Singh SP. Synthesis of zinc oxide by sol-gel method and to study it's structural properties. AIP Conf Proc. 2020;2220:020184. doi: 10.1063/5.0001593.

15. Dulta K, Agceli GK, Chauhan P, Chauhan PK. Biogenic production and characterization of CuO nanoparticles by carica papaya leaves and its biocompatibility applications. J Inorg Organomet Polym. 2021;31(4):1846-57. doi: 10.1007/s10904-020-01837-7.

16. Diwan R, Shinde A, Malpathak N. Phytochemical composition and antioxidant potential of Ruta graveolens L. *in vitro* culture lines. J Bot. 2012;2012:1-6. doi: 10.1155/2012/685427.

17. Akbarian M, Mahjoub S, Elahi SM, Zabihi E, Tashakkorian H. Appraisal of the biological aspect of Zinc oxide nanoparticles prepared using extract of Camellia sinensis L. Mater Res Express. 2019 Sep 26;6(9):095022. doi: 10.1088/2053-1591/ab2c49.

18. Rajan Abhinaya S, Padmini R. Biofabrication of zinc oxide nanoparticles using Pterocarpus marsupium and its biomedical applications. Asian J Pharm Clin Res 2018;12(1). doi: 10.22159/ajpcr.2018.v12i1.28682.

19. Kowsalya E, MosaChristas K, Jaquline CRI, Balashanmugam P, Devasena T. Gold nanoparticles induced apoptosis via oxidative stress and mitochondrial dysfunctions in MCF-7 breast cancer cells. Applied Organom Chemis. 2021;35(1). doi: 10.1002/aoc.6071.

20. Erdogan MK, Agca CA, Askın H. Quercetin and luteolin improve the anticancer effects of 5-fluorouracil in human colorectal adenocarcinoma *in vitro* model: a mechanistic insight. Nutr Cancer. 2022 Mar;74(2):660-76. doi: 10.1080/01635581.2021.1900301, PMID 34309458.

21. Pate KP, Safier PS. Chemical metrology methods for CMP quality. Adv Chem Mech Planarization (CMP). 2016:299-325. doi: 10.1016/B978-0-08-100165-3.00012-7.

22. Das B, Dash SK, Mandal D, Ghosh T, Chattopadhyay S, Tripathy S. Green synthesized silver nanoparticles destroy multidrug resistant bacteria via reactive oxygen species mediated membrane damage. Arab J Chem. 2017;10(6):862-76. doi: 10.1016/j.arabjc.2015.08.008.

23. Tulasi SL, Swamy AVVS, Pavani P, Subhashini V. Green synthesis of zinc oxide nanoparticles using schrebera swietenioides roxb., aqueous leaf extract and investigation of its effect on seed germination and plant growth on pigeon pea (Cajanus cajan Linn.). Int J App Pharm. 2022;14(2):193-9. doi: 10.22159/ijap.2022v14i2.43696.

24. MH, PR. Phytosynthesis and characterization of silver nanoparticles from Ruellia tuberosa (L.): effect of physicochemical parameters. Asian J Pharm Clin Res. 2021;14(12):31-8. doi: 10.22159/ajpcr.2021.v14i12.42020.

25. AbdElhady MM. Preparation and characterization of chitosan/zinc oxide nanoparticles for imparting antimicrobial and UV protection to cotton fabric. Int J Carbohydr Chem. 2012;2012:1-6. doi: 10.1155/2012/840591.

26. Giri PK, Bhattacharyya S, Chetia B, Kumari S, Singh DK, Iyer PK. High-yield chemical synthesis of hexagonal ZnO nanoparticles and nanorods with excellent optical properties. J Nanosci Nanotechnol. 2012 Jan;12(1):201-6. doi: 10.1166/jnn.2012.5113, PMID 22523966.

27. Phaniendra A, Jestadi DB, Periyasamy L. Free radicals: properties, sources, targets, and their implication in various diseases. Indian J Clin Biochem. 2015 Jan;30(1):11-26. doi: 10.1007/s12291-014-0446-0, PMID 25646037.

28. Meulmeester FL, Luo J, Martens LG, Mills K, van Heemst D, Noordam R. Antioxidant supplementation in oxidative stress-related diseases: what have we learned from studies on alpha-tocopherol? Antioxidants (Basel). 2022 Nov 24;11(12):2322. doi: 10.3390/antiox11122322, PMID 36552530.

29. Lobo V, Patil A, Phatak A, Chandra N. Free radicals, antioxidants and functional foods: impact on human health. Pharmacogn Rev. 2010 Jul;4(8):118-26. doi: 10.4103/0973-7847.70902, PMID 22228951.

30. Pereira RM, Andrades NE, Paulino N, Sawaya AC, Eberlin MN, Marcucci MC. Synthesis and characterization of a metal complex containing naringin and Cu, and its antioxidant, antimicrobial, antiinflammatory and tumor cell cytotoxicity. Molecules. 2007 Sep 30;12(7):1352-66. doi: 10.3390/12071352, PMID 17909491.

31. Ananthalakshmi R, Rajarathinam SRX, Sadiq AM. Antioxidant activity of ZnO nanoparticles synthesized using luffa acutangula peel extract. Res J Pharm Technol. 2019;12(4):1569-72. doi: 10.5958/0974-360X.2019.00260.9.

32. Ginouves M, Carme B, Couppie P, Prevot G. Comparison of tetrazolium salt assays for evaluation of drug activity against Leishmania spp. J Clin Microbiol. 2014 Jun;52(6):2131-8. doi: 10.1128/JCM.00201-14, PMID 24719447.

33. Escobar ML, Echeverria OM, Vazquez Nin GH. Necrosis as programmed cell death. In: Cell death–autophagy, apoptosis and necrosis. Intech Open; 2012. p. 61-81. doi: 10.5772/61483.

34. Umamaheswari A, Prabu SL, John SA, Puratchikody A. Green synthesis of zinc oxide nanoparticles using leaf extracts of raphanus sativus var. Longipinnatus and evaluation of their anticancer property in A549 cell lines. Biotechnol Rep (Amst). 2021 Dec;29:e00595. doi: 10.1016/j.btre.2021.e00595, PMID 33659193.

35. Stabrauskiene J, Kopustinskiene DM, Lazauskas R, Bernatoniene J. Naringin and naringenin: their mechanisms of action and the potential anticancer activities. Biomedicines. 2022 Jun 23;10(7):1686. doi: 10.3390/biomedicines10071686, PMID 35884991.